

Ordered metal nanostructure self-assembly using metal-organic frameworks as templates

Benjamin W. Jacobs,¹ Ronald J. T. Houk,¹ Stephen D. House,² Ian M. Robertson,² A. Alec Talin,³ Mark D. Allendorf^{1,*}

1. Sandia National Laboratories, Livermore, California, 94550, USA

*email: mdallen@sandia.gov

2. Department of Materials Science and Engineering, University of Illinois, Urbana, Illinois, 61801, USA

3. Center for Nanoscience and Technology, National Institute of Standards and Technology, Gaithersburg, Maryland, 20899, USA

Synthesis of metal nanoparticles and nanowires with controlled size and aspect ratio is an active research field,¹⁻⁴ motivated by the unique and useful optical, magnetic, and catalytic properties of these nanostructures. Here, we demonstrate a method in which nanoporous metal-organic frameworks (MOFs) loaded with silver serve as templates for ordered silver nanostructures. Exposure to an electron beam breaks down the template, leading to rapid silver coalescence. The geometric and chemical structure of the MOF, as well as the extent of metal loading, determine whether nanoparticles or nanowires are formed and define their size and orientation. Nanowires with diameters as small as 4 nm and aspect ratios > 125 can be formed, opening a path to self-assembled nanostructure design and synthesis that overcomes the limitations of existing templating methods. This method is relatively simple, compatible with many materials, and proceeds by a distinct template-directed growth mechanism. Since MOFs offer an unprecedented level of synthetic flexibility combined with highly uniform porosity as a result of their crystalline structure, this approach opens a promising new route for synthesis of self-assembled, ordered inorganic nanostructures.

The unique, size-dependent properties of metallic nanoparticles make these materials attractive for variety of applications in optics, magnetics, electronics, catalysis and bio/medicine.¹ Assembly of these into two or three-dimensional nanostructures, leads to additional novel properties that stem from collective optical and electronic behavior. These properties, in principle, can be tuned by controlling the nanoparticle areal or spatial arrangement and can depend on the characteristics of the supporting matrix.^{2,3} A common strategy for forming 2-D or 3-D assemblies of nanostructures is by template-directed synthesis.^{8,9} Soft templates, such as inverse micelles,¹⁰ typically have a defined structure that only persists in solution and are easily deformed. Hard templates, on the other hand, such as anodized aluminum oxide,¹¹ mesoporous silica,¹² or diblock copolymers,¹³ maintain their shape in the solid state, and may or may not be removed depending on the desired application. The basic mechanism of

template-directed synthesis is the same: growth occurs over a defined area or volume, which we generically refer to as a 'pore', that determines the dimensions, spacing, and placement of individual nanostructures. The factors currently limit the effectiveness of templated growth: 1) pore dimensions below 5 nm are difficult to achieve by either top-down or bottom-up methods, 2) the nanoparticle surface is typically covered with ligands or encased in a solid matrix thus limiting applications such as catalysis or sensing, and 3) the resulting spatial arrangement of the pores is essentially limited to close-packed or in some cases square patterns. A simple, but versatile bottom-up method is needed for next-generation applications that addresses these limitations and is compatible with many different materials to enable flexible, reproducible, and scalable nanostructure fabrication.

Metal organic frameworks (MOFs) are a new class of crystalline, nanoporous material that are attracting considerable interest because of their unprecedented degree of synthetic flexibility. The pore size, shape, and chemistry of MOFs can be precisely tuned, and an extensive library of synthesized structures already exists. MOFs are hybrid materials in which metal ions or clusters are connected by electron-donating "linker" groups to create a networked structure with rigid pores. This porosity creates the potential to introduce non-native functionality to a given structure by infusing the accessible volume with a second material. Both vapor-phase and solution methods developed by Fischer and others have been used to infiltrate MOFs with Pd, Pt, Au, Cu, Fe, ZnO, TiO₂, and Ru,¹⁴⁻¹⁷ while retaining the MOF crystal structure. Other approaches, including the use of redox active frameworks to create Ag and Au nanoparticles¹⁸ and using the MOF itself as starting material for nanoparticle synthesis,¹⁹ have also been demonstrated.

We recently discovered that infiltrating MOFs with an ethanolic solution of AgNO₃ creates very small, sterically and chemically stabilised nanoclusters evenly distributed within the framework (Ag@MOF).²⁰ Electron paramagnetic resonance (EPR) measurements indicate clusters as small as Ag₃ can form. Elemental analysis of the infiltrated MOFs indicates that average cluster sizes range from Ag₂ to

Ag₂₀. Exposure to a transmission electron microscope (TEM) beam quickly breaks down the framework, leading to Ag coalescence and the formation of larger nanoparticles. This suggests that deliberate exposure of Ag@MOFs to an electron beam can be used as a bottom-up self-assembly method to fabricate metal nanostructures. In this report we show that ordered arrays of both Ag nanowires and nanoparticles are possible using this method. The rate of template breakdown and subsequent Ag coalescence depend on the crystal structure of the host MOF and determine whether Ag nanowire arrays or Ag nanoparticles with narrow size distributions form.

Three different MOFs were selected for this investigation to systematically probe the relationship between pore structure and Ag nanostructure formation (Table S1): Cu(BTC), MIL-68(In), and MOF-508. Cu(BTC), which has Cu(II) atoms connected to benzenetricarboxylate (BTC) linkers, is expected to yield arrays of Ag nanoparticles due to its primitive cubic structure with enclosed spherical pore cavities connected by smaller pore apertures.²¹ In contrast, the two types of 1-D pores within MIL-68(In) (1.8 nm and 1 nm diameter, respectively) appear to be well suited to the formation of nanowires.²² This MOF is composed of 1-D chains of In atoms connected by 1,4-benzenedicarboxylate (BDC) linkers to form a Kagomé-type lattice. The third structure, MOF-508, has an interpenetrated crystal lattice with five 1-D pores that are also geometrically well suited to nanowire formation. All three MOFs have metal-carboxylate linkages in at least two of the three crystallographic dimensions, creating common pore chemistry. MOF-508 adds an additional dimension, however. In this case, two-dimensional sheets formed by Zn₂(OAc)₄ paddle-wheel units and BDC linkers in the xz plane are linked to one another by 4,4'-dipyridyl (bipy) ligands.²³ This gives MOF-508 reversible structural flexibility, which is characteristic of a number of MOFs. The “open” MOF-508 structure occurs in the presence of solvent, while the “closed” form occurs when the solvent is desorbed from the pores. Based on elemental analysis the Ag loadings for Ag@MIL-68(In) and Ag@MOF-508 are 3.5 Ag atoms/nm³ and 0.5 Ag atoms/nm³ for Ag@Cu(BTC).

When Ag@Cu(BTC) is exposed to the TEM electron beam only Ag nanoparticles form. As seen in Fig. 1, Ag particles (confirmed by the *fcc* selected area electron diffraction, SAED, pattern) with an average diameter of 4.3 ± 1.1 nm are observed, while no 1-D nanostructures are seen. As mentioned above, the Ag loading in Cu(BTC) is low, so there are not many Ag atoms in close proximity to each other that can coalesce. In addition, the lack of constant-diameter 1-D pores and the small apertures between pore cavities are not favorable for Ag diffusion. These factors effectively confine Ag and limit particle growth.

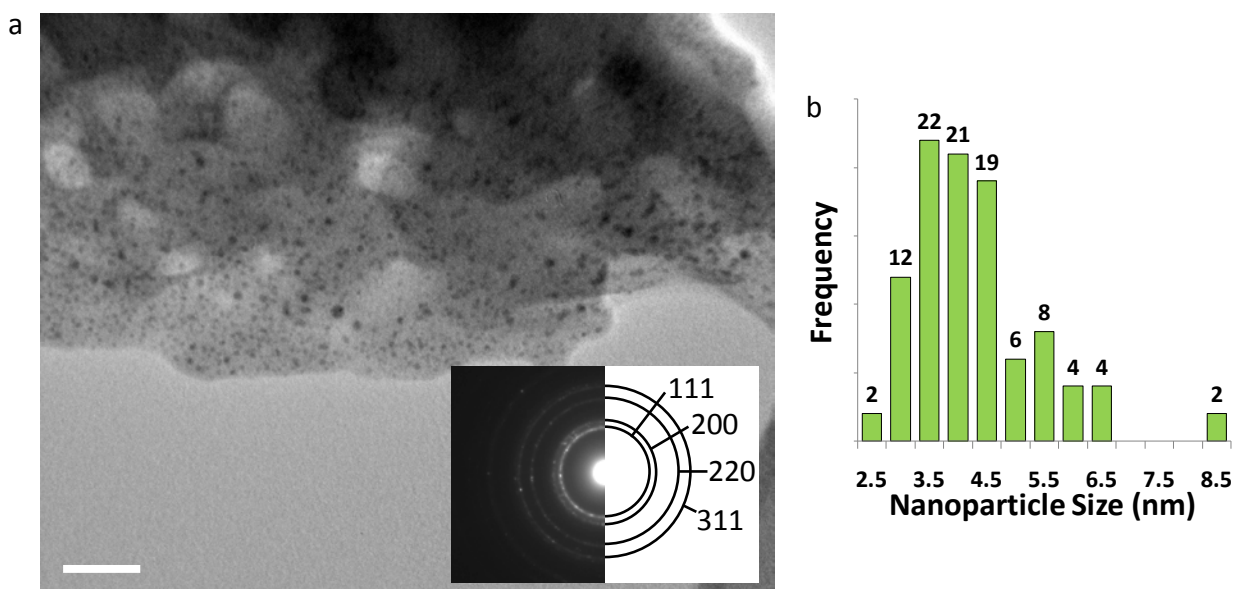


Figure 1. Silver nanostructure formation in Ag@Cu(BTC). a) TEM image of Cu(BTC) after 1 minute exposure to the electron beam. Dark contrast spots indicate Ag nanoparticles. Scale bar is 50 nm. The inset is a diffraction pattern that was solved for the *fcc* structure of Ag. b) Size distribution histogram of the Ag nanoparticles that form after electron beam exposure in Ag@Cu(BTC).

The 1-D channels of MIL-68(In) produce nanowires as well as nanoparticles when the Ag-loaded template is exposed to the electron beam. Distinct lines of dark contrast, indicated by the arrows in Figs. 2b and 2d, suggest the presence of nanowires. Although Ag nanoparticles with an average size of 2.9 ± 0.47 nm (Fig. 2c) are prevalent throughout Ag@MIL-68(In), video obtained as the crystal is exposed to the beam clearly demonstrates the strong directionality imposed by the crystal environment that leads to nanowire formation (video S1). Frames from the video (Figs. 2a and 2b) show that the breakdown and

subsequent formation of nanoparticles and nanowires occurs within 10 s of beam exposure.

Interestingly, however, nanowires can also form at crystalline defects, as seen in Fig. S1 and video S2.

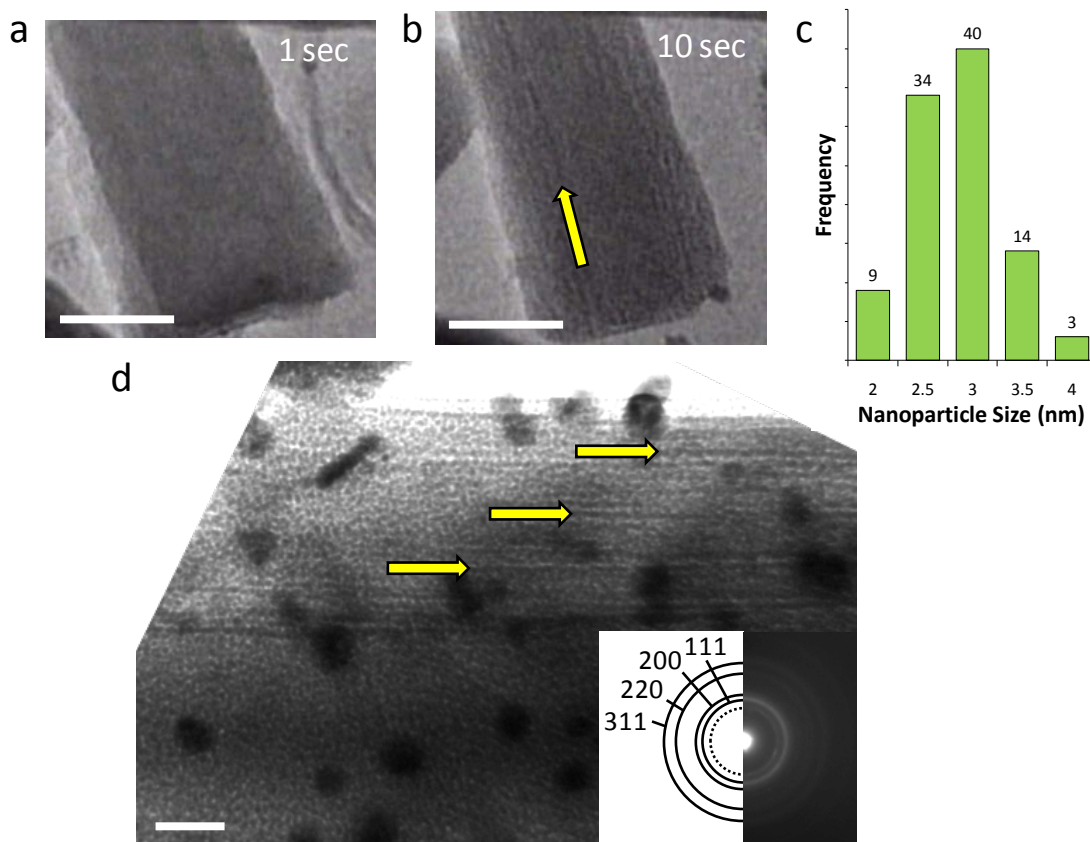


Figure 2. Silver nanostructure formation in Ag@MIL-68(In). a) TEM image of Ag infiltrated MIL-68(In) after 1 s in the electron beam. b) TEM image of the same area in (a) after 10 s in the electron beam. The yellow arrow indicates the location of a Ag nanowire that formed in the framework. c) Histogram showing the size distribution of Ag nanoparticles that form in Ag@MIL-68(In). d) TEM image showing Ag nanowires that form in Ag@MIL-68(In). Three Ag nanowires are indicated by the yellow arrows. The larger dark contrast spots are coalesced Ag nanoparticles on the surface of the MOF that form during the infiltration process. The inset shows a diffraction pattern that was solved for the *fcc* structure of Ag, and the dotted circle is diffraction from metallic indium. All scale bars are 50 nm.

Highly ordered Ag nanowires readily form when Ag@MOF-508 is exposed to the electron beam.

The TEM image in Fig. 3a reveals Ag nanowires oriented along the axes of 1-D pores in MOF-508. These nanowires are ≈ 4 nm to 13 nm in diameter and are oriented at 125° relative to each other. Such arrays are found throughout multiple samples and conform to the same geometric orientation (Fig. S2). Arrows at the bottom of Fig. 3a indicate that parallel nanowires form at approximately 50 nm intervals. A high-resolution TEM (HRTEM) image of an individual nanowire (Fig. 3b) shows that the structure is

polycrystalline. Silver nanoparticles with a narrow size distribution ($3.9 \text{ nm} \pm 0.69 \text{ nm}$; Fig. 3c) also form in addition to nanowires and are uniformly distributed throughout the framework.

We note that the SAED patterns of none of the Ag@MOF indicate the formation of metal oxides (ZnO, CuO, or In_2O_3). No evidence of metallic zinc is seen in the SAED pattern of Ag@MOF-508 either. However, trace amounts of indium metal are evident in the pattern from Ag@MIL-68(In). We cannot determine if metallic copper forms when Ag@Cu(BTC) is exposed to the beam because its diffraction pattern overlaps that of Ag. This phenomenon currently under investigation and will be the subject of a future report.

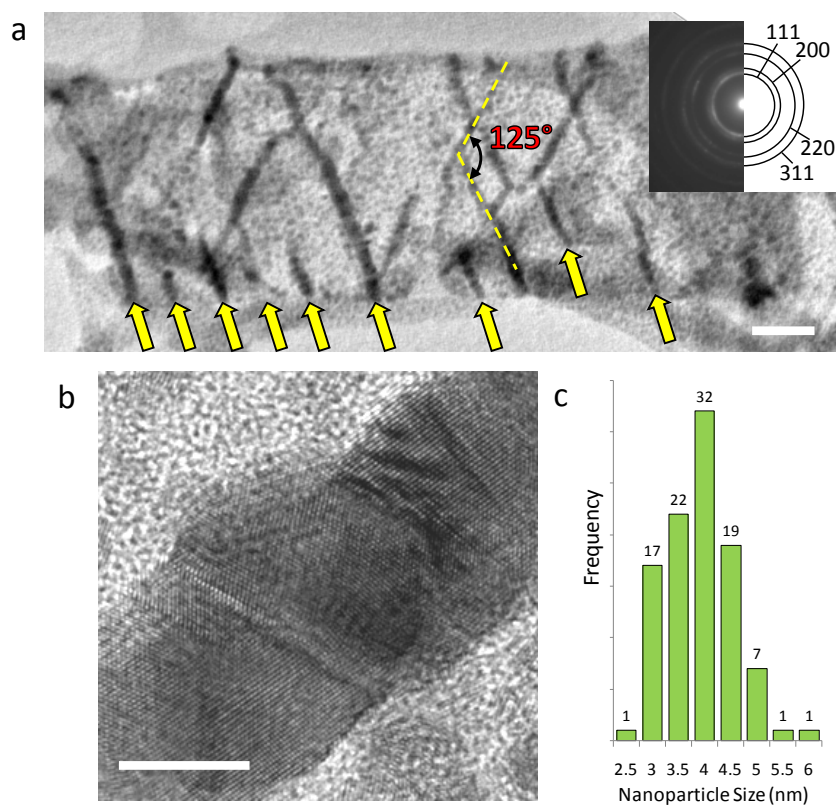


Figure 3. Silver nanostructure formation in Ag@MOF-508. a) TEM image showing nanowire array that formed in the electron beam. The nanowires are oriented 125° relative to each other. Arrows at the bottom of the figure indicate where parallel nanowires have formed. More nanowires that form in this direction, suggesting that this pore is chemically preferred for nanowire formation. The scale bar is 50 nm. The inset is an electron diffraction pattern that was solved for the fcc structure of Ag. b) High resolution TEM image of an Ag nanowire that formed in Ag@MOF-508. The scale bar is 5 nm. d) Silver nanoparticle size distribution.

Bond scission by means of secondary electron generation from the electron beam is the most likely cause of MOF breakdown and Ag coalescence. However, electron beam-induced heating can also damage organic materials, so we used Bethe's formula to estimate the increase in local temperature during nanostructure formation.²⁴ This analysis indicates that the sample temperature increases only ≈ 10 K above room temperature during the experiment, not enough to damage the MOF (see supplementary information for details). Alternatively, electron ionization mass spectra of carboxylic acids show that dehydroxylation and decarboxylation are the first and most abundant fragmentation events (Fig. S3). Fourier transform infrared spectroscopy (FTIR) indicates the infiltrated Ag is located near the metal-carboxylate bonds in each framework (Fig. S4).²⁰ Thus, nanoparticle destabilization is likely to occur quickly, releasing the small clusters to diffuse and coalesce. The remaining hydrocarbon fragments polymerize, forming carbonaceous material (Fig. S5).

The morphology of the observed Ag nanostructures can be linked to the chemical environment within the pores. This is evident in the case of MOF-508 (Figs. 4a-c), an interpenetrated network of two sublattices, in which there are five distinct 1-D pores large enough to accommodate a Ag atom. Three of these pores (Fig. S6) are unfavorable for nanowire formation because solvent evacuation following AgNO_3 infiltration transforms MOF-508 into its "closed" form, as evidenced by powder XRD (Fig. S7), rendering these pores discontinuous. These closed pores are likely nucleation sites for the nanoparticles that are observed. The remaining two pore types, oriented along the green (xz pore) and red (x pore) lines in Figs. 4a and 4b, respectively, remain open after solvent evacuation (Fig. S8) and are the likely hosts for nanowire formation. These two channels intersect at an angle of $\approx 128^\circ$ (Fig. 4c), which closely matches the observed angle between nanowires (Fig. 3a). Although both pores have nearly the same dimensions (0.41 nm x 0.41 nm) and are larger than the Van der Waals diameter of a Ag atom (0.34 nm), we expect the bidentate coordination of Ag enabled by short (0.37 nm) carboxylate-carboxylate distances across the xz pore to be particularly favorable for nanowire formation (Fig. S9). Indeed, TEM

images strongly suggest (e.g., Figs. 3a and S2) there is a preferred pore for nanowire formation (arrows in Fig. 3a). In contrast, the larger carboxylate separation in the x pore (0.78 nm) should allow predominantly monodentate binding (Fig. S9). Both pores have carboxylate spacings large enough to accommodate the Ag₃ clusters observed by EPR (0.6 nm along the length of the xz pore and 0.61 nm across the x pore).²⁰

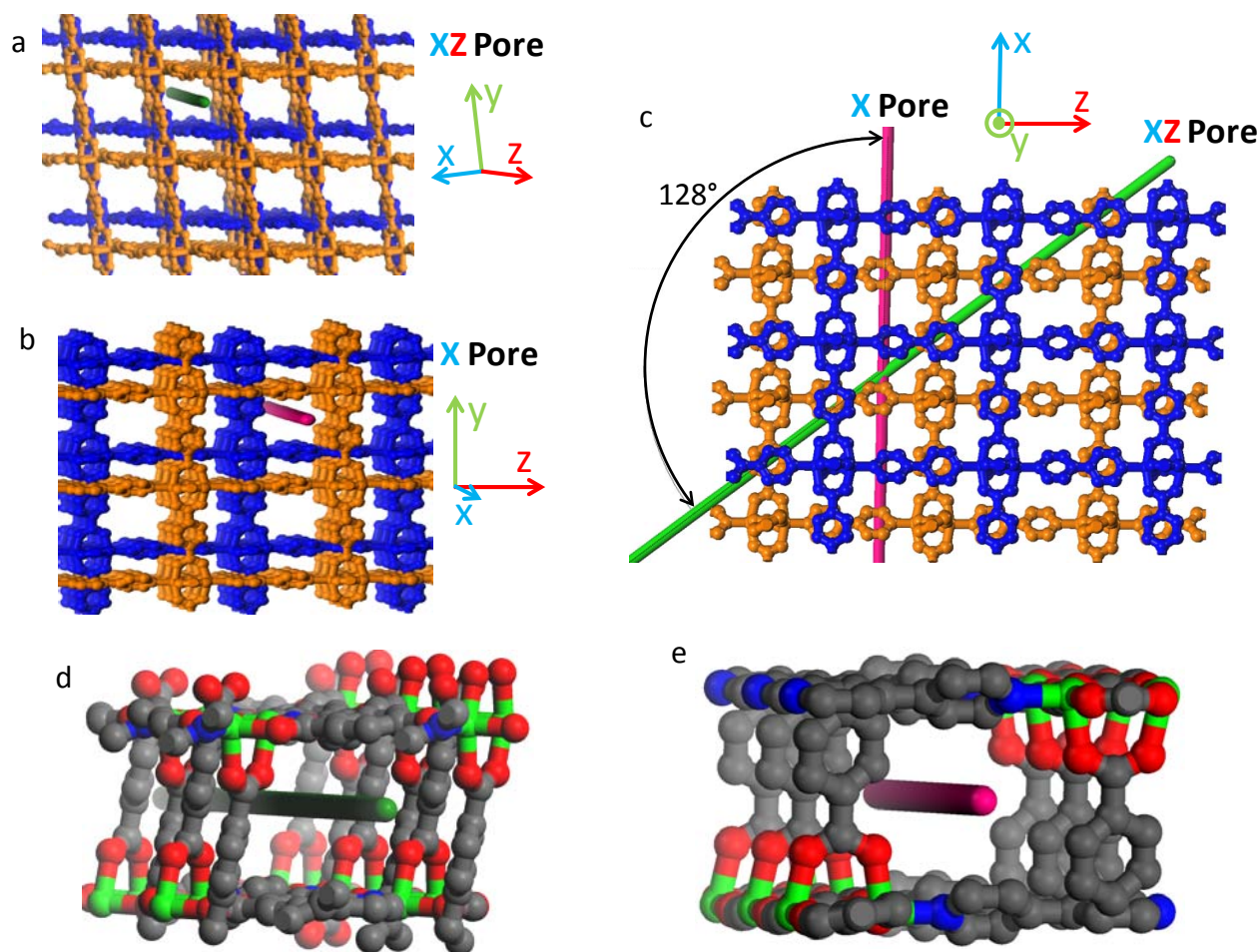


Figure 4. Dependence of Ag nanostructure formation on MOF-508 crystal structure. The interpenetrated sublattices of MOF-508 are distinguished by the blue and orange color. a) MOF-508 crystal oriented along the xz direction. The green line shows the orientation of a 1-D pore (xz pore) favorable for nanowire formation. b) MOF-508 crystal oriented 128° relative to (a) along the x direction. The red line shows the orientation of the other 1-D pore (x pore) favorable for nanowire formation. c) MOF-508 crystal oriented perpendicular to pores in (a) and (b), the angle between pores is 128°. d) Close up of the xz pore. Gray: carbon; red: oxygen; blue: nitrogen; green: zinc. e) Close up of the pore from (b). The color coding is the same as in (d).

The chemical and geometric environment of the pores in MIL-68(In) and Cu(BTC) make it clear why nanowires are less likely to form in these templates. The 1-D pores of MIL-68(In) are much larger

than those in MOF-508 and contain many oxygen sites that can stabilize Ag (Fig. 5a). However, the pore walls are defined by the aromatic rings of the carboxylate linkers (Fig. S10), leaving little space for Ag to diffuse from adjacent pores and leading primarily to nanoparticle formation. This is in stark contrast to MOF-508. Here, the crystal structure is much more open than MIL-68(In), allowing Ag to readily diffuse in three dimensions. Radial diffusion in Cu(BTC) is similarly inhibited by the enclosed, isotropic pore structure and high number of carboxylate oxygen ions surrounding the pore (Fig. 5b). Thus, Cu(BTC) acts as a zero-dimensional template rather than a 1-D template.

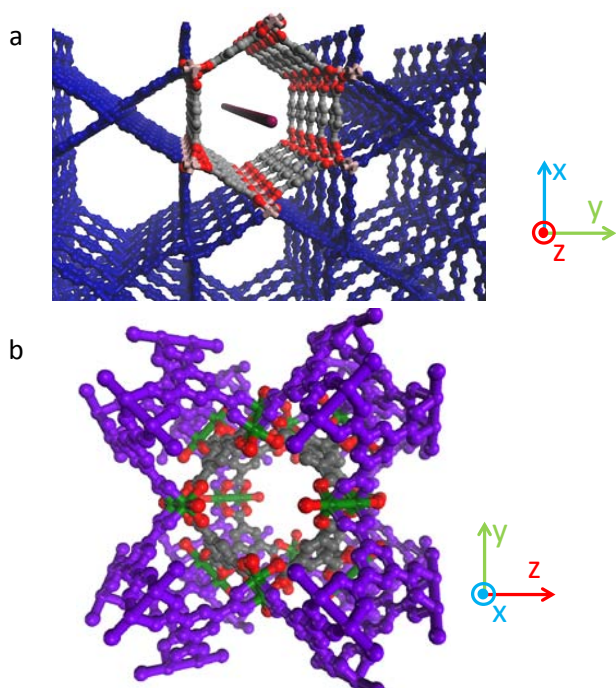


Figure 5. Dependence of MIL-68(In) and Cu(BTC) crystal structure on Ag nanostructure formation, with atoms surrounding the pore highlighted. Gray: carbon; red: oxygen; peach: indium; green: copper. a) The red line shows the orientation of the 1-D pores in MIL-68(In). The larger of the two pore types is highlighted. b) Crystal structure of Cu(BTC), in which approximately spherical pores are connected by smaller pore openings.

Two timescales are important in Ag nanostructure formation: the nucleation time and the time available for growth prior to MOF collapse, which effectively freezes the structure. Since the thermodynamic driving force to condensation is very large for Ag, we expect the Ag nanostructure nucleation rate to be determined by the local density of Ag within the pore, which at the relatively low loadings used here is controlled by the local density of stabilizing oxygen atoms. On this basis, the

nucleation rates should be similar for the three MOFs, which all have roughly the same number of oxygen atoms (10 oxygen atoms /nm³). Using the mobility reported for Ag atoms in viscous epoxy polymers (3×10^{-12} cm²/s),²⁵ we estimate that a Ag atom can diffuse 10 nm in ≈ 80 ms. Our TEM video images suggest the following times are necessary for framework collapse under the electron beam current density used here (10.3 A/m²): Cu(BTC) ≈ 1 s; MIL-68(In) ≈ 2 s; and MOF-508 ≈ 5 s. Thus, Ag has more time to diffuse and coalesce in MOF-508 than in the other two MOFs, leading to larger nanostructures spaced further apart. The reason for the enhanced robustness of MOF-508 relative to the other two may result from the fact that the “closed” form of this structure is denser and has a higher number of inter-linker interactions, making the two open channels more stable than they would be in a less dense structure such as Cu(BTC).

Elemental analysis of the infiltrated MOFs provides additional quantitative insight into the dynamics of Ag nanostructure formation in MOF-508. Using the average loading in MOF-508 (3.5 Ag atoms/nm³) and the unit cell volume (1.68 nm³), we calculate that a 10-nm diameter nanowire 50 nm long would require Ag from $\approx 70,000$ neighboring unit cells. Assuming uniform radial Ag diffusion toward the nanowire, this corresponds to diffusion from unit cells up to ≈ 19 nm away from the nanowire axis. Therefore, the core-to-core nanowire spacing should be ≈ 38 nm. This agrees reasonably well with the relatively constant 50 nm spacing between nanowires observed in the MOF-508 array. It appears that nanowire formation occurs not only by atom-by-atom growth, but also by nanocluster agglomeration. The HRTEM results (Fig. 1b) show that Ag nanowires are polycrystalline with grain sizes similar to Ag nanoparticles that form (2 nm – 5 nm diameter). This implies that nanowire formation is a two step process. In the first step, Ag nanoclusters nucleate and grow to form primary nanoparticles 1 nm to 5 nm in diameter within 0.1 s – 1 s. In the second step, the primary particles diffuse and coalesce into continuous nanowires. This occurs on a longer time scale, because larger Ag particles are not as mobile as single Ag atoms or small molecular-scale clusters. Based on the video images (Fig. S11; video S3),

nanoparticles in MOF-508 can diffuse up to 5 nm in just 4 seconds, which is less than the template lifetime (~ 5 s). We estimate the nanoparticle diffusion constant based on these values to be 1.6×10^{-14} cm^2/s , consistent with previous reports.²⁶ Nanowire growth in Ag@MIL-68(In) occurs by a similar mechanism in those instances when nanoparticles coalesce before the framework collapses.

In summary, the bottom-up self assembly approach described here produces arrays of Ag nanoparticles or nanowires with dimensions as small as 2 nm and nanowire aspect ratios > 125 . Morphology can be controlled by judicious choice of the MOF and the extent of metal loading. A major advantage of this method over other templates is that the uniform nanoporosity imposed by the MOF crystal structure enables nanostructure feature sizes $\ll 10$ nm to be produced. Moreover, unlike many other templates, in which size alone determines the properties of the resulting structures, MOFs provide both chemical and steric constraints that can be tailored to achieve specific patterns, sizes and shapes. Although the size of the exposed area in our proof-of-concept experiments was limited by the diameter of the TEM beam, both high-resolution writing and broad-area exposure are possible using currently available instrumentation. Extension of this method to other metals should be straightforward using previously reported infiltration techniques. Demonstrated layer-by-layer MOF surface growth on planar substrates enables infiltration and patterning that can be integrated into devices.²⁷ Finally, fabrication of 3-D architectures is plausible, since epitaxial growth of layered structures composed of MOFs with different pore sizes has been shown.²⁸

Methods

MOF Synthesis. All reagents were purchased from Sigma-Aldrich or Acros Organics, and solvents were purchased from Fisher Scientific and used without purification.

Cu(BTC): Copper(II) nitrate trihydrate (2.9 g, 12 mmol, 1.5 eq.) is dissolved in 25 mL of nanopure water. Trimesic acid (1.68 g, 8 mmol, 1 eq.) is dissolved separately in 25 mL of 200 proof ethanol. The solutions are mixed in a pyrex media jar and capped tightly. The reaction vessel is sealed in a thick-walled PTFE jar for secondary containment, and the apparatus is placed in an oven at 110 °C for 24 hours. The blue crystalline precipitate is filtered and washed 3x with ethanol, 3x with water, and allowed to air dry for 3 days. The reaction yield is 75% based on copper. The crystals are activated under low vacuum (10^{-1} Torr) at 180 °C overnight. Note that Cu(BTC) is very hygroscopic and re-exposure to ambient atmosphere will cause rapid re-adsorption of water vapor. The powder x-ray diffraction pattern is consistent with the literature. Activated Cu(BTC) was found to have a Langmuir surface area of 1352 m^2/g .

MOF-508: Zinc(II) nitrate hexahydrate (703 mg, 2.3 mmol, 1 eq.), terephthalic acid (393 mg, 2.3 mmol, 1 eq.), and 4,4'-dipyridyl (185 mg, 1.2 mmol, 0.5 eq.) are dissolved in 200 mL of 1:1 ethanol/DMF in a pyrex media jar. The jar is capped tightly and placed in a 90 °C oven for 24 hours. Upon completion, the white crystalline powder is filtered and washed with 3 x 30 mL DMF then 2 x 30 mL hexanes. The yield as synthesized based on zinc is 82%. The framework is activated under low vacuum (10 Pa) at 180 °C overnight. Both the as synthesized and activated powder x-ray diffraction patterns are consistent with the literature.²³ Activated MOF-508 was found to have a Langmuir surface area of 592 m²/g.

MIL-68(In): Indium(III) nitrate pentahydrate (2.45 g, 6.3 mmol, 1 eq.) and terephthalic acid (1.2 g, 7 mmol, 1.15 eq.) are dissolved in 30 mL DMF in a glass media jar with sonication and heating. The reaction vessel is tightly capped and placed in an oven at 100 °C for 2 days. The MOF precipitates in large (200 μm) crystallites, which are allowed to cool and are then filtered and washed with DMF. Yield based on Indium is 80%. The MOF is activated under low vacuum (10 Pa) at 180 °C overnight and gives an x-ray powder diffraction pattern consistent with the literature.²² Activated MIL-68(In) was found to have a Langmuir surface area of 956 m²/g.

Ag Infiltration. In a typical infiltration experiment, ≈100 mg of the chosen MOF was activated under low vacuum (10⁻¹ Torr) at 180 °C for 16 hours, then further evacuated at room temperature on a schlenk apparatus (10⁻² Torr.) Ag(I) nitrate (256 mg, 1.5 mmol) was dissolved in 500 μL nanopure water then diluted to 3 mL with 200-proof ethanol to generate a 0.5 M AgNO₃ solution in 5:1 ethanol/water. The Ag salt solution was then cannulated into a glass vial containing the evacuated MOF to generate a slurry. The reaction vessel was backfilled with N₂, sonicated for 2 minutes to ensure thorough mixing, then placed on a shaker and agitated 16 hours at an angular velocity of 250 min⁻¹. Following thorough washing to remove excess salt or unbound Ag particles, the samples were reactivated at 180 °C at 10 Pa for 16 hours. Alternatively, for best results in generating nanowires, reactivation of the Ag@MOF materials is carried out under vacuum at room temperature for 2 days.

TEM sample preparation, electron beam exposure and electron tomography. All MOF samples were suspended in ethanol and sonicated for 30 s. Copper TEM grids with a lacey carbon support film were dipped into the suspension and allowed to dry. The grids were placed in a vacuum chamber with a roughing pump overnight. A JEOL 2010F field-emission TEM operating at 200 kV was used to initiate nanostructure growth and analyze the resulting material morphology. The current density of the electron beam was held constant at 10.3 A/m² when observing nanostructure formation in the MOFs. The current density is minimized to reduce the speed at which the MOFs break down, but sufficiently bright to visualize the break down and coalescence effects in real time.

Acknowledgements. This work was supported by the Laboratory Directed Research and Development Program at Sandia National Laboratories and at the University of Illinois by the Metal Hydrides Center of Excellence, Office of Energy Efficiency and Renewable Energy, U.S. Department of Energy under grant No. DE-FC36-05GO15064. Sandia is a multiprogram laboratory operated by Sandia Corporation, a Lockheed Martin Company, for the United States Department of Energy's National Nuclear Security Administration under Contract DE-AC04-94AL85000. Certain commercial equipment, instruments, or materials are identified in this paper to foster understanding. Such identification does not imply recommendation or endorsement by the National Institute of Standards and Technology, nor does it imply that the materials or equipment identified are necessarily the best available for the purpose.

References

- 1 Burda, C., Chen, X. B., Narayanan, R. & El-Sayed, M. A. Chemistry and properties of nanocrystals of different shapes. *Chemical Reviews* **105**, 1025-1102, doi:10.1021/cr030063a (2005).
- 2 Ozin, G. A. & Arsenault, A. C. *Nanochemistry: a chemical approach to nanomaterials.* (Royal Society of Chemistry, 2005).
- 3 Fan, H. Y. *et al.* Self-assembly of ordered, robust, three-dimensional gold nanocrystal/silica arrays. *Science* **304**, 567-571 (2004).

- 4 Brinker, C. J. Evaporation-induced self-assembly: Functional nanostructures made easy. *Mrs Bulletin* **29**, 631-640 (2004).
- 5 Talapin, D. V., Lee, J.-S., Kovalenko, M. V. & Shevchenko, E. V. Prospects of colloidal nanocrystals for electronic and optoelectronic applications. *Chem Rev* **110**, 389-458 (2010).
- 6 Claridge, S. A. *et al.* Cluster-Assembled Materials. *ACS Nano* **3**, 244-255, doi:10.1021/nn800820e (2009).
- 7 Talapin, D. V. *et al.* Quasicrystalline order in self-assembled binary nanoparticle superlattices. *Nature* **461**, 964-967, doi:10.1038/nature08439 (2009).
- 8 Zhang, Z. S., Zhang, S. Y. & Li, W. R. Templates and their applications in synthesis of nanomaterials. *Progress in Chemistry* **16**, 26-34 (2004).
- 9 Bronstein, L. M. Nanoparticles made in mesoporous solids. *Colloid Chemistry* **1** **226**, 55-89, doi:10.1007/b10824 (2003).
- 10 Huo, Q. S. *et al.* GENERALIZED SYNTHESIS OF PERIODIC SURFACTANT INORGANIC COMPOSITE-MATERIALS. *Nature* **368**, 317-321 (1994).
- 11 Martin, C. R. NANOMATERIALS - A MEMBRANE-BASED SYNTHETIC APPROACH. *Science* **266**, 1961-1966 (1994).
- 12 Li, G. T. *et al.* Gram-scale synthesis of submicrometer-long polythiophene wires in mesoporous silica matrices. *Angewandte Chemie-International Edition* **42**, 3818-3821, doi:10.1002/anie.200351158 (2003).
- 13 Ruiz, R. *et al.* Density multiplication and improved lithography by directed block copolymer assembly. *Science* **321**, 936-939, doi:10.1126/science.1157626 (2008).
- 14 Turner, S. *et al.* Direct imaging of loaded metal-organic framework materials (metal@MOF-5). *Chemistry of Materials* **20**, 5622-5627, doi:10.1021/cm801165s (2008).
- 15 Muller, M., Zhang, X. N., Wang, Y. M. & Fischer, R. A. Nanometer-sized titania hosted inside MOF-5. *Chemical Communications*, 119-121, doi:10.1039/b814241f (2009).
- 16 Esken, D., Zhang, X., Lebedev, O. I., Schroder, F. & Fischer, R. A. Pd@MOF-5: limitations of gas-phase infiltration and solution impregnation of Zn₄O(bdc)(3) (MOF-5) with metal-organic palladium precursors for loading with Pd nanoparticles. *Journal of Materials Chemistry* **19**, 1314-1319, doi:10.1039/b815977g (2009).
- 17 Muller, M., Lebedev, O. I. & Fischer, R. A. Gas-phase loading of Zn₄O(btb)(2) (MOF-177) with organometallic CVD-precursors: inclusion compounds of the type LnM (a)@MOF-177 and the formation of Cu and Pd nanoparticles inside MOF-177. *Journal of Materials Chemistry* **18**, 5274-5281, doi:10.1039/b810989c (2008).
- 18 Moon, H. R., Kim, J. H. & Suh, M. P. Redox-active porous metal-organic framework producing silver nanoparticles from Ag⁺ ions at room temperature. *Angewandte Chemie-International Edition* **44**, 1261-1265, doi:10.1002/anie.200461408 (2005).
- 19 Liu, B. *et al.* Converting cobalt oxide subunits in cobalt metal-organic framework into agglomerated Co₃O₄ nanoparticles as an electrode material for lithium ion battery. *Journal of Power Sources* **195**, 857-861, doi:10.1016/j.jpowsour.2009.08.058 (2010).
- 20 Houk, R. J. T. *et al.* Silver Cluster Formation, Dynamics, and Chemistry in Metal-Organic Frameworks. *Nano Letters* **9**, 3413-3418, doi:10.1021/nl901397k (2009).
- 21 Chui, S. S. Y., Lo, S. M. F., Charmant, J. P. H., Orpen, A. G. & Williams, I. D. A chemically functionalizable nanoporous material Cu-3(TMA)(2)(H₂O)(3) (n). *Science* **283**, 1148-1150 (1999).
- 22 Volkringer, C. *et al.* The Kagome Topology of the Gallium and Indium Metal-Organic Framework Types with a MIL-68 Structure: Synthesis, XRD, Solid-State NMR Characterizations, and Hydrogen Adsorption. *Inorganic Chemistry* **47**, 11892-11901, doi:10.1021/ic801624v (2008).

- 23 Chen, B. L. *et al.* A microporous metal-organic framework for gas-chromatographic separation of alkanes. *Angewandte Chemie-International Edition* **45**, 1390-1393, doi:10.1002/anie.200502844 (2006).
- 24 Zhenyu, T. & Yancai, H. An empirical energy loss equation of electrons. *Scanning* **24**, 46-51 (2002).
- 25 Gaddy, G. A. *et al.* Light-induced formation of silver particles and clusters in crosslinked PVA/PAA films. *Journal of Physical Chemistry B* **108**, 14850-14857, doi:10.1021/jp0497561 (2004).
- 26 Akamatsu, K., Tsuboi, N., Hatakenaka, Y. & Deki, S. In situ spectroscopic and microscopic study on dispersion of Ag nanoparticles in polymer thin films. *Journal of Physical Chemistry B* **104**, 10168-10173 (2000).
- 27 Fischer, R. A. & Woll, C. Layer-by-Layer Liquid-Phase Epitaxy of Crystalline Coordination Polymers at Surfaces. *Angewandte Chemie-International Edition* **48**, 6205-6208, doi:10.1002/anie.200901090 (2009).
- 28 Furukawa, S. *et al.* Heterogeneously Hybridized Porous Coordination Polymer Crystals: Fabrication of Heterometallic Core-Shell Single Crystals with an In-Plane Rotational Epitaxial Relationship. *Angewandte Chemie-International Edition* **48**, 1766-1770, doi:10.1002/anie.200804836 (2009).